

C₂H, HC₃N and HNC observations in OMC-2/3 *

Qiang Liu^{1,2}, Ji Yang¹, Yan Sun¹ and Ye Xu¹

¹ Purple Mountain Observatory, Chinese Academy of Science, Nanjing 210008, China
qiangliu@pmo.ac.cn

² Graduate University of Chinese Academy of Sciences, Beijing 100049, China

Received 2011 January 8; accepted 2011 January 16

Abstract For the first time, the OMC-2/3 region was mapped in C₂H (1–0), HC₃N (10–9) and HNC (1–0) lines. In general, the emissions from all the three molecular species reveal an extended filamentary structure. The distribution of C₂H cores almost follows that of the 1300 μm condensations, which might suggest that C₂H is a good tracer to study the core structure of molecular clouds. The core masses traced by HNC are rather flat, ranging from 18.8 to 49.5 M_⊙, while also presenting a large span for those from C₂H, ranging from 6.4 to 36.0 M_⊙. The line widths of both HNC and C₂H look very similar, and both are wider than that of HC₃N. The line widths of the three lines are all wider than those from dark clouds, implying that the former is more active than the latter, and has larger turbulence caused by winds and UV radiation from the surrounding massive stars.

Key words: ISM: abundances — ISM: individual (Orion Molecular Clouds) — ISM: molecules — stars: formation

1 INTRODUCTION

The Orion A molecular cloud, at a heliocentric distance of 450 pc (Genzel & Stutzki 1989; it is worth noting that Menten et al. 2007 recently measured the parallax distance and gave a value of 420 pc), is one of the nearest active high mass star-forming regions. To the northern end of Orion A, the J-shaped OMC-2/3 region is regarded as one of the best sites to study both “clustered” and triggered star formation due to its near proximity. Therefore, OMC-2/3 aroused great interest since its discovery and was comprehensively studied recently at a variety of wavelengths and with a variety of molecular species.

Chini et al. (1997) identified at least 21 compact 1300 μm dust continuum condensations in OMC-2/3, with 16 of them embedded in OMC-2 and the others in OMC-3. They suggested that the condensations in OMC-3 with $L_{\text{bol}}/L_{\text{SMM}} < 70$ are Class 0 objects and thus represent an earlier stage of evolution. The 3.6 cm free-free emission revealed 14 sources, of which seven sources coincide well with the 1300 μm condensations, yet no relation was found between the 3.6 cm radio continuum and 1300 μm (Reipurth et al. 1999). Williams et al. (2003) observed CO(1–0) toward this region and identified nine protostellar outflows.

Dense cores in this region were well studied in many molecular species, e.g. CS and C¹⁸O (Castets & Langer 1995), NH₃ (Cesaroni & Wilson 1994), HCO⁺ and CO (Aso et al. 2000). The

* Supported by the National Natural Science Foundation of China.

chemical evolution of OMC-2/3 was also widely studied in a variety of molecular species, in particular the complex molecule species, such as CH₃OH, HC₃N, and CCS. Johnstone et al. (2003) studied the astrochemistry of OMC-2/3 in H₂CO, CH₃OH, etc., and found a trend that hotter cores are more likely to have higher CO, H₂CO, CH₃OH, and CS abundance. Tatematsu et al. (2008) observed N₂H⁺, HC₃N and CCS toward Orion A and found that the N-bearing molecules seem to be more intense in OMC-2. Tatematsu et al. (2010) investigated Orion A in CCS, HC₃N, DNC, and HN¹³C and detected CCS emission in OMC-3 for the first time. They also proposed that star formation activity seems to be responsible for the enhancement of HC₃N intensity.

We mapped the OMC-2/3 region in C₂H, HC₃N, and HNC. These molecular lines were widely studied in dark clouds and were commonly accepted as good tracers of the physical condition and chemical evolution of dense cores. C₂H was first detected in the interstellar medium by Tucker et al. (1974). It has since been detected in a variety of interstellar environments (Wootten et al. 1980, Huggins et al. 1984). Recently, Beuther et al. (2008) further revealed that C₂H can be found in cases from the earliest infrared dark clouds (IRDCs) to the later evolutionary stage of ultra-compact HII regions and explained that it was replenished at the core edges by elemental carbon from CO being dissociated by the interstellar UV photons. Due to its small rotation constant, HC₃N creates many transitions that are easily detectable in molecular clouds (Vanden Bout et al. 1983). Moreover, the transitions are likely to be optically thin, so it was also an excellent dense gas indicator. However, its mechanism of formation is still not very clear. Woon & Herbst (1997) proposed that it originated from the reaction between CN and C₂H₂. Szczepanski et al. (2005) gave a pathway of formation for HC₃N from a C₃ carbon cluster and ammonia. Observations of these molecular lines can help us understand the chemistry of HC₃N. HNC molecules are considered to be relevant for the formation mechanism of cyanopolynes (HC_{2n+1}N) in future work.

2 OBSERVATIONS

The observations were made during 2010 March and July with the PMO 13.7 m millimeter-wave telescope at Delingha, China. The observation center ($\alpha = 05^{\text{h}}35^{\text{m}}26.71^{\text{s}}$, $\delta = -05^{\circ}10'04''$, equinox=2000.0) was adopted from Chini et al. (1997), the location of FIR 4, which is associated with the strongest 3.6 cm emission (Reipurth et al. 1999). The HNC(1–0), HC₃N(10–9) and C₂H(1–0) were mapped over a 10' by 23' region with a grid spacing of 60''. The detailed observation log is listed in Table 1 (Tucker et al. 1974).

Table 1 Observed Transitions and Rest Frequencies

Molecule	Transition	ν (MHz)	Relative intensity	B_0 (MHz)	μ (D)
C ₂ H	$J = 3/2 \rightarrow 1/2$ $F = 1 \rightarrow 1$	87 284.38	4.25	43 474	0.8
	$J = 3/2 \rightarrow 1/2$ $F = 2 \rightarrow 1$	87 317.05	41.67		
	$J = 3/2 \rightarrow 1/2$ $F = 1 \rightarrow 0$	87 328.70	20.75		
	$J = 1/2 \rightarrow 1/2$ $F = 1 \rightarrow 1$	87 402.10	20.75		
	$J = 1/2 \rightarrow 1/2$ $F = 0 \rightarrow 1$	87 407.23	8.33		
	$J = 1/2 \rightarrow 1/2$ $F = 1 \rightarrow 0$	87 446.42	4.25		
HC ₃ N	$J = 10 \rightarrow 9$	90 978.99		4 549	3.72
HNC	$J = 1 \rightarrow 0$	90 663.59		45 332	3.05

An SIS receiver with a noise temperature of 75–145 K (DSB) was used. The back end was a Fast Fourier Transform Spectrometer (FFTS) having 16 384 channels with a bandwidth of 1000 MHz and effective spectral resolution of 61.0 kHz (0.20 km s⁻¹). With the 1000 MHz bandwidth, HNC(1–0) and HC₃N(10–9) were received simultaneously. The position-switch mode was used. The system temperatures were about 200–300 K during the observations. The pointing accuracy was checked by regular observations of point sources and was estimated to be better than 9''. The main beam size

was about 60'' at 115 GHz. The typical on-source time for each position was about 5 min. The main-beam efficiency θ_{mb} was estimated by comparing the radiation temperatures of calibration sources S140, NGC2264 and Orion A with the NRAO 11 m results (e.g. Huggins et al. 1984; Morris et al. 1976).

All the data were reduced by using the GILDAS software. We performed linear baseline subtractions to most spectra. At the velocity resolution of 0.2 km s^{-1} the typical rms noise level was about 0.2 K in T_{A}^* .

3 RESULTS AND DISCUSSION

3.1 Spectra and Maps

Figure 1 shows the spectra of the observation center. The intensity scale is given in T_{R}^* in all figures from this study. Here all six hyperfine components of C₂H $N = 1 \rightarrow 0$ are presented. The line profiles of both HNC and HC₃N show a very symmetric Gaussian profile at this position.

Figure 2 shows the velocity integrated intensity contour and grey-scale maps for the strongest components $J = 3/2 \rightarrow 1/2 F = 2 \rightarrow 1$ of C₂H, HC₃N and HNC. The integrated velocity ranges from 8 to 14 km s⁻¹ for all observed lines. The 1300 μm cores identified by Chini et al. (1997) are marked by pluses in Panel a. It is evident that the distribution of 1300 μm cores shows the most resemblance to that of our C₂H cores. In general, the emissions from all the three molecular species revealed an extended filamentary structure. More than one condensation was detected in both OMC-2 and OMC-3. One exception is the HC₃N emission in OMC-3, which is almost negligible and shows very marginal detection ($\sim 3\sigma$). The location of each core was derived from the channel maps

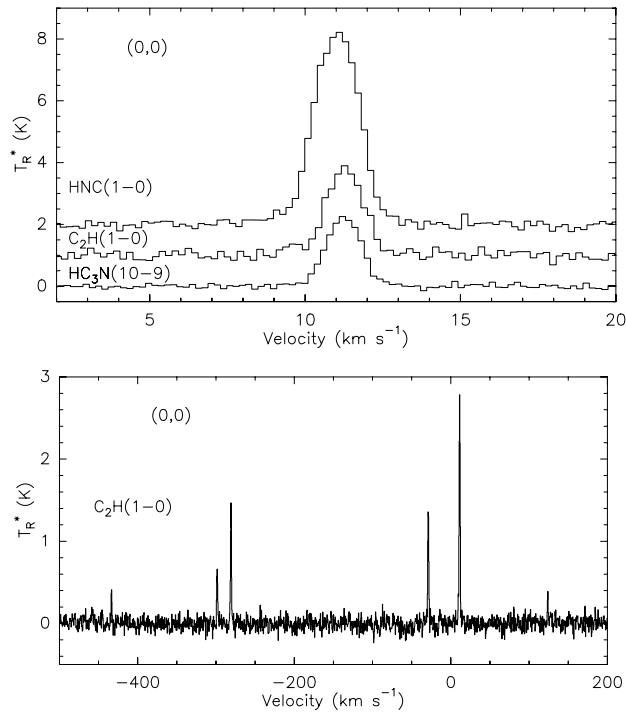


Fig. 1 *Top:* spectra towards (0'', 0''); *Bottom:* six hyperfine components of C₂H $N = 1 \rightarrow 0$.

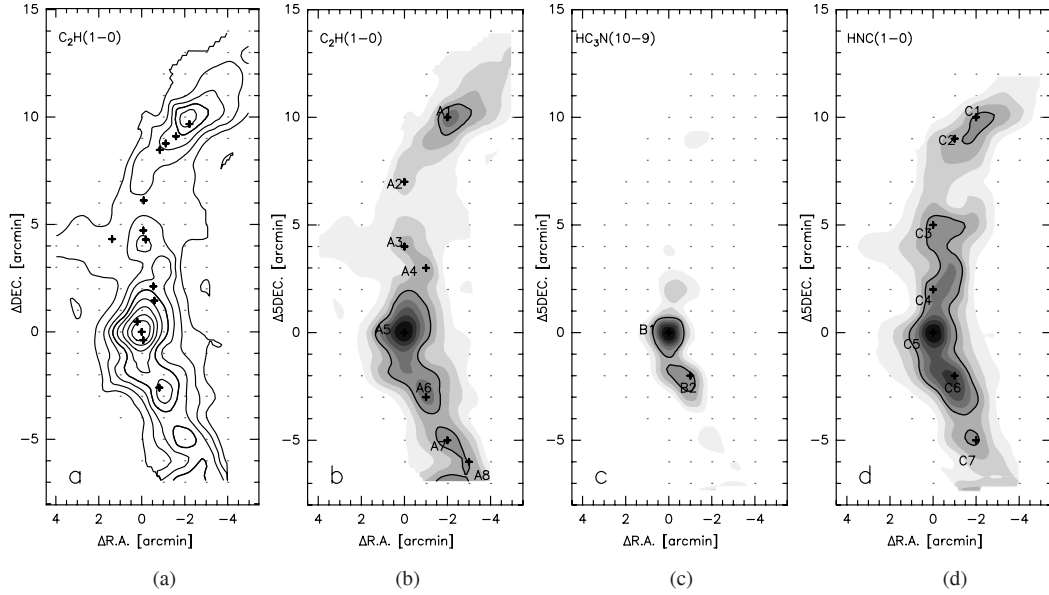


Fig. 2 (a) velocity integrated intensity contour map of the C_2H $J = 3/2 \rightarrow 1/2$ $F = 2 \rightarrow 1$. The contour levels are $4.367 \text{ K km s}^{-1} \times (2, 3, 4, 5, 6, 7, 8, 9)$. Pluses represent the $1300 \mu\text{m}$ condensations identified by Chini et al. (1997). (b)–(d) velocity integrated intensity contour and grey-scale maps of the C_2H $J = 3/2 \rightarrow 1/2$ $F = 2 \rightarrow 1$, $HC_3N(10-9)$ and $HNC(1-0)$. The contour levels are $4.367 \text{ K km s}^{-1} \times (2, 3, 4, 5, 6, 7, 8, 9)$, $1.785 \text{ K km s}^{-1} \times (3, 4, 5, 6, 7, 8, 9)$, and $11.2 \text{ K km s}^{-1} \times (2, 3, 4, 5, 6, 7, 8, 9)$, respectively. Pluses mark the positions of all cores identified in this study.

by eye and by applying a threshold of 5σ in two adjacent channels. To improve the signal-to-noise ratio, the channel width was resampled to be 0.5 km s^{-1} . Finally, we identified at least eight C_2H $J = 3/2 \rightarrow 1/2$ $F = 2 \rightarrow 1$ cores indicated by A1–A8, two $HC_3N(10-9)$ cores indicated by B1 and B2, and seven $HNC(1-0)$ cores indicated by (C1–C7) in OMC-2/3. The location of each core is marked by a plus sign in Figure 2. The size of the core is characterized by the nominal core radius R after beam deconvolution, which was calculated by

$$R = \left[\frac{A}{\pi} - \left(\frac{\text{HPBW}}{2} \right)^2 \right]^{1/2}, \quad (1)$$

where A is the measured area within the contour of half peak intensity. The derived location and size of each core is summarized in Table 2, which also lists the corresponding Gaussian fitting results for the main components of C_2H , HC_3N and HNC , including the line center velocity, the line widths and the bright temperature. The shape of most cores is elongated due to the compression from the surrounding medium. The radii of C_2H cores range from 0.12 to 0.17 pc with a mean value of 0.14 pc, while HNC cores range from 0.15 to 0.21 pc with a mean value of 0.17 pc. The size of the two $HC_3N(10-9)$ cores is much smaller, only 0.08 and 0.09 pc, about half the value of radius for both HNC and C_2H cores. In OMC-2, the radius of the $C^{32}S(2-1)$ core was found to be about 0.1 pc with a resolution of $53''$ (Castets & Langer 1995), and that of the $CS(1-0)$ core was found to be 0.18 pc with a resolution of $35''$ (Tatematsu et al. 1993). The discrepancy in radius traced by different molecular species might reflect that $HC_3N(10-9)$ and $C^{32}S(2-1)$, and perhaps $C_2H(1-0)$, trace a much denser region than $HNC(1-0)$ and $CS(1-0)$.

Table 2 Cores' Parameters

No	offset (arcmin)	offset (arcmin)	R (arcmin)	R (pc)	V_{LSR} (km s ⁻¹)	ΔV (km s ⁻¹)	T_{mb} (K)
A1	-2	10	1.34	0.17	10.9±0.04	1.8±0.08	1.4
A2	0	7	0.95	0.12	10.9±0.04	1.2±0.10	1.2
A3	0	4	1.18	0.15	11.6±0.04	1.4±0.12	1.1
A4	-1	3	0.92	0.12	11.3±0.06	1.7±0.15	1.0
A5	0	0	1.32	0.17	11.3±0.02	1.4±0.04	2.8
A6	-1	-3	0.94	0.12	10.7±0.03	1.5±0.08	1.6
A7	-2	-5	1.00	0.13	10.6±0.04	1.5±0.11	1.5
A8	-3	-6	1.01	0.13	10.4±0.02	0.85±0.07	1.8
B1	0	0	0.62	0.08	11.2±0.01	1.3±0.02	2.3
B2	-1	-2	0.86	0.11	11.0±0.02	1.1±0.06	1.4
C1	-2	10	1.17	0.15	10.7±0.02	1.9±0.04	2.9
C2	-1	9	1.35	0.18	10.9±0.01	1.5±0.03	3.3
C3	0	5	1.63	0.21	11.2±0.01	1.1±0.02	5.1
C4	0	2	1.27	0.17	11.2±0.01	1.5±0.02	4.2
C5	0	0	1.17	0.15	11.0±0.01	1.7±0.01	6.4
C6	-1	-2	1.35	0.18	10.8±0.01	1.3±0.02	6.3
C7	-2	-5	1.14	0.15	10.4±0.01	1.6±0.03	3.3

3.2 Radial Velocity and Line Width

The velocities along the line of sight listed in Table 2 show good agreement among C₂H, HC₃N and HNC cores. The V_{LSR} ranges from 10.4 to 11.6 km s⁻¹ for C₂H (1–0) cores, and 10.4 to 11.2 km s⁻¹ for HNC(1–0) cores. The V_{LSR} values of the two HC₃N(10–9) cores are all around 11.0 km s⁻¹. By comparing with the V_{LSR} derived from C¹⁸O (2–1) and C³²S (2–1) observations (Castets et al. 1995), we found that the V_{LSR} derived from different molecular species are very coherent.

In the north-south direction, a velocity gradient across OMC-2 is apparent in both HNC and C₂H, however, that is not the case for OMC-3 (see Table 2). Figure 3 shows the position-velocity diagram, for the HNC (left) and C₂H (middle) along $\Delta\text{R.A.} = -1$, and for HC₃N (right) along $\Delta\text{R.A.} = 0$. The velocity gradient in OMC-2 was obvious. The previous study also found that the V_{LSR} increased gradually from south to north along the Orion A filaments (e.g. Bally et al. 1987). One reasonable explanation for its origin was the compression and acceleration from the adjacent Orion OB I associations (Bally et al. 1987).

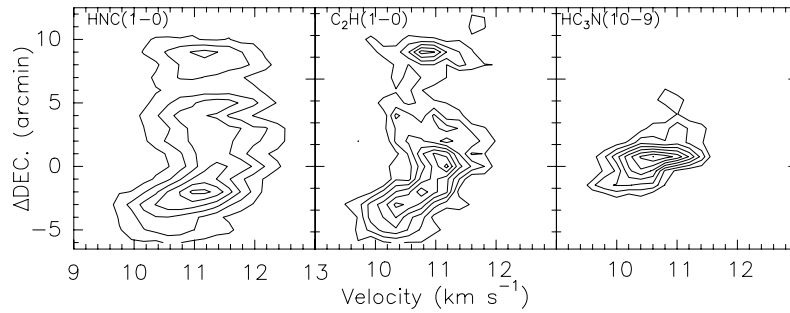


Fig. 3 Position-velocity diagram for the HNC (*left*) and C₂H (*middle*) along $\Delta\text{R.A.} = -1$ and for HC₃N (*right*) along $\Delta\text{R.A.} = 0$.

The line widths of C₂H(1–0), HNC(1–0), and HC₃N(10–9) range from 0.85 to 1.8 km s^{−1}, 1.1 to 1.9 km s^{−1} and 1.1 to 1.3 km s^{−1}, respectively. The line widths of both HNC and C₂H look very similar, and both are wider than those of HC₃N. This indicates that HC₃N traces a cooler region. As previously mentioned, HC₃N can trace a much denser and more central region of a cloud than HNC and C₂H, which might be the reason why HC₃N shows the narrowest line width.

Many factors contribute to the line width of a specific molecular specie. Among them, the contribution from thermal broadening is about 0.2 km s^{−1}, so in our case non-thermal broadening is mainly attributed to the line width. In dark clouds, the typical line width is about 0.4–1.0 km s^{−1} for C₂H(1–0) (Wootten et al. 1980), 0.1–0.4 km s^{−1} for HC₃N(10–9), and 0.5–0.7 km s^{−1} for HNC(1–0) (e.g. in TMC-1; Churchwell et al. 1984), which are all much narrower than those of the OMC-2/3 region. This suggests that OMC-2/3 is more active than dark clouds, and has a larger turbulence caused by winds and UV radiation from the surrounding massive stars.

3.3 Column Density and Cores' Masses

We perform hyperfine structure (HFS) fitting to C₂H (1–0), to estimate the excitation temperature T_{ex} , which was given as $T_{\text{ex}}=T_{\text{ant}} + T_{\text{bg}}$, and optical depth τ_{TOT} , which was given as $\tau_{\text{TOT}}=\tau_{\text{main}}/0.4167$ (Padovani et al. 2009).

The total gas column density along the line of sight was calculated under the assumption that each tracer is optically thin, in Local Thermodynamic Equilibrium (LTE), and can be expressed as (Scoville et al. 1986),

$$N = \frac{3k}{8\pi^3 B \mu^2} \frac{e^{hB J_l(J_l+1)/kT_{\text{ex}}}}{J_l + 1} \frac{T_{\text{ex}} + hB/3k}{1 - e^{-h\nu/kT_{\text{ex}}}} \int \tau_{\nu} d\nu, \quad (2)$$

where B is the rotational constant, μ is a permanent dipole moment, and J_l is the rotational quantum number of the lower state in the observed transition (Table 1). The excitation temperatures of HC₃N and HNC were assumed to be 20 K in OMC-2 and 15 K in OMC-3, which were taken from NH₃ observations of Wilson et al. (1999).

The H₂ column density $N(\text{H}_2)$ was estimated by assuming $N(\text{C}_2\text{H})/N(\text{H}_2)=5.3 \times 10^{-9}$, $N(\text{HC}_3\text{N})/N(\text{H}_2)=1.3 \times 10^{-10}$, and $N(\text{HNC})/N(\text{H}_2)=5.3 \times 10^{-10}$ (Blake et al. 1987). Core masses

Table 3 Cores' Properties

No	T_{ex} (K)	τ_{TOT}	N (cm ^{−2})	$N(\text{H}_2)$ (cm ^{−2})	$n(\text{H}_2)$ (cm ^{−3})	M (M_{\odot})	M_{vir} (M_{\odot})	M_{vir}/M
A1	5.1	1.2±0.33	1.2×10^{14}	2.3×10^{22}	2.2×10^4	31.6	64.0	2.0
A2	4.8	1.2±0.54	7.5×10^{13}	1.4×10^{22}	1.9×10^4	9.6	30.1	2.7
A3	7.0	0.4±0.42	4.8×10^{13}	9.1×10^{21}	1.0×10^4	9.9	43.9	4.0
A4	8.9	0.2±1.62	4.2×10^{13}	7.9×10^{21}	1.1×10^4	5.6	42.6	7.1
A5	13.9	0.4±0.15	1.4×10^{14}	2.6×10^{22}	2.5×10^4	36.0	49.7	1.2
A6	8.8	0.4±0.28	7.2×10^{13}	1.4×10^{22}	1.9×10^4	9.6	37.6	3.7
A7	11.7	0.2±0.60	5.7×10^{13}	1.1×10^{22}	1.4×10^4	9.0	40.8	4.2
A8	13.5	0.2±0.46	4.1×10^{13}	7.7×10^{21}	1.0×10^4	6.4	23.1	3.3
B1			1.2×10^{13}	9.2×10^{22}	18.6×10^4	27.9	21.8	0.8
B2			6.1×10^{12}	4.7×10^{22}	6.9×10^4	26.9	25.4	0.9
C1			1.3×10^{13}	2.5×10^{22}	2.7×10^4	26.7	59.6	2.2
C2			1.2×10^{13}	2.3×10^{22}	2.1×10^4	35.8	56.4	1.6
C3			1.1×10^{13}	2.1×10^{22}	1.6×10^4	43.4	48.3	1.1
C4			1.2×10^{13}	2.3×10^{22}	2.2×10^4	31.6	53.3	1.7
C5			2.2×10^{13}	4.2×10^{22}	4.5×10^4	44.4	53.3	1.2
C6			1.7×10^{13}	3.2×10^{22}	2.9×10^4	49.5	48.9	1.0
C7			9.8×10^{12}	1.8×10^{22}	1.9×10^4	18.8	50.2	2.7

were calculated by equation $M = m_{\text{H}} X \times N(\text{H}_2) \times (\pi R^2)$ where X is the ratio of total gas mass to hydrogen mass, which is about 1.36. The virial mass M_{vir} was calculated by equation $M_{\text{vir}}(M_{\odot}) = 210R(\text{pc}) \delta v(\text{km s}^{-1})$. All derived physical parameters are tabulated in Table 3.

An interesting result is that the core masses traced by HNC are rather flat, ranging from 18.8 to 49.5 M_{\odot} . By contrast, those traced by C₂H are steep, ranging from 6.4 to 36.0 M_{\odot} . On the whole, OMC-2 is more massive than OMC-3. The average masses for C₂H, HC₃N and HNC cores are 14.7, 35.7 and 23.6 M_{\odot} , respectively. The core masses we derived here were strongly dependent on the adopted abundance values and therefore likely have a large uncertainty. The average virial masses of C₂H, HC₃N and HNC cores are 41.5, 23.6 and 52.7 M_{\odot} , respectively. M_{vir}/M listed in Table 3 is inversely proportional to the M term, which is consistent with the conclusion of Loren (1989) that low mass clumps are more likely to deviate from virial equilibrium.

4 SUMMARY

We first mapped the OMC-2/3 region in C₂H(1–0), HC₃N(10–9) and HNC(1–0) by using the PMO 13.7 m telescope. Our main results are summarized as follows:

- (1) The distribution of C₂H cores shows the most resemblance to that of the 1300 μm condensations, which might suggest that C₂H is a good tracer to study the structure of molecular clouds.
- (2) HC₃N shows the narrowest line width, while the widths of both HNC and C₂H share a very similar distribution. In general, the line width of the three observed lines presented here is wider than that of the dark cloud. This might imply that OMC-2/3 is more active than the dark cloud, and has larger turbulence caused by winds and UV radiation from the surrounding massive stars.
- (3) The core masses traced by HNC are rather flat, ranging from 18.8 to 49.5 M_{\odot} , while, by contrast, those traced by C₂H are steep, ranging from 6.4 to 36.0 M_{\odot} .

Acknowledgements We would like to thank the 13.7 m Observatory staff for their support during the observation. This work was supported by the National Natural Science Foundation of China (Grant Nos. 11003046, 11073054, 10733030 and 10621303), and the National Basic Research Program of China (973 Program, Grant 2007CB815403).

References

- Aso, Y., Tatematsu, K., Sekimoto, Y., et al. 2000, *ApJS*, 131, 465
 Bally, J., Lanber, W. D., Stark, A. A., & Wilson, R. W. 1987, *ApJ*, 312, L45
 Beuther, H., Semenov, D., Henning, T., & Linz, H. 2008, *ApJ*, 675, L33
 Blake, G. A., Sutton, E. C., Masson, C. R., & Phillips, T. G. 1987, *ApJ*, 315, 621
 Castets, A., & Langer, W. D. 1995, *A&A*, 294, 835
 Cesaroni, R., & Wilson, T. L. 1994, *A&A*, 281, 209
 Chini, R., Reipurth, B., Ward-Thompson, D., et al. 1997, *ApJ*, 474, L135
 Churchwell, E., Nash, A. G., & Walmsley, C. M. 1984, *ApJ*, 287, 681
 Genzel, R., & Stutzki, J. 1989, *ARA&A*, 27, 41
 Huggins, P. J., Carlson, W. J., & Kinney, A. L. 1984, *A&A*, 133, 347
 Johnstone, D., Boonman, A. M. S., & van Dishoeck, E. F. 2003, *A&A*, 412, 157
 Loren, R. B. 1989, *ApJ*, 338, 902
 Menten, K. M., Reid, M. J., Forbrich, J., & Brunthaler, A. 2007, *A&A*, 474, 515
 Morris, M., Turner, B. E., Palmer, P., & Zuckerman, B. 1976, *ApJ*, 205, 82
 Padovani, M., Walmsley, C. M., Tafalla, M., Galli, D., & Müller, H. S. P. 2009, *A&A*, 505, 1199
 Reipurth, B., Rodríguez, L. F., & Chini, R. 1999, *AJ*, 118, 983
 Scoville, N. Z., Sargent, A. I., Sanders, D. B., et al. 1986, *ApJ*, 303, 416

- Szczepanski, J., Wang, H., Doughty, B., Cole, J., & Vala, M. 2005, *ApJ*, 626, L69
- Tatematsu, K., Hirota, T., Kandori, R., & Umemoto, T. 2010, arXiv:1010.4939
- Tatematsu, K., Kandori, R., Umemoto, T., & Sekimoto, Y. 2008, *PASJ*, 60, 407
- Tatematsu, K., Umemoto, T., Kameya, O., et al. 1993, *ApJ*, 404, 643
- Tucker, K. D., Kutner, M. L., & Thaddeus, P. 1974, *ApJ*, 193, L115
- Vanden Bout, P. A., Loren, R. B., Snell, R. L., & Wootten, A. 1983, *ApJ*, 271, 161
- Williams, J. P., Plambeck, R. L., & Heyer, M. H. 2003, *ApJ*, 591, 1025
- Wilson, T. L., Mauersberger, R., Gensheimer, P. D., Muders, D., & Bieging, J. H. 1999, *ApJ*, 525, 343
- Woon, D. E., & Herbst, E. 1997, *ApJ*, 477, 204
- Wootten, A., Bozyan, E. P., Garrett, D. B., Loren, R. B., & Snell, R. L. 1980, *ApJ*, 239, 844